

A CALCULATIONAL APPROACH TO IONIZATION  
SPECTROMETER DESIGN\*

T. A. Gabriel  
Oak Ridge National Laboratory  
Oak Ridge, Tennessee, 37830

I. INTRODUCTION

Many factors contribute to the design and overall performance of an ionization spectrometer.<sup>1-4</sup> These factors include the conditions under which the spectrometer is to be used, the required performance, the development of the hadronic and electromagnetic cascades, leakage and binding energies, saturation effects of densely ionizing particles, nonuniform light collection, sampling fluctuations, etc. In this paper, the calculational procedures developed at Oak Ridge National Laboratory that have been applied to many spectrometer designs and that include many of the influencing factors in spectrometer design are discussed. The incident-particle types which can be considered with some generality are protons, neutrons, pions, muons, electrons, positrons, and gamma rays. Charged kaons can also be considered but with less generality. The incident-particle energy range can extend into the hundreds of GeV range. The calculations have been verified by comparison with experimental data but only up to approximately 30 GeV. Some comparisons with experimental data will also be discussed and presented so that the flexibility of the calculational methods can be demonstrated.

---

\*This research was funded by the U. S. Energy Research and Development Administration under contract with the Union Carbide Corporation.

## II. METHOD OF CALCULATION

The three-dimensional, multimedia high-energy nucleon-meson transport code HETC<sup>5</sup> is used to obtain a detailed description of the nucleon-meson cascade produced in the spectrometer. This Monte Carlo code takes into account the slowing down of charged particles (via the continuous slowing-down approximation), the decay of charged pions and muons, nonelastic nucleon- and charged-pion-nucleus (excluding hydrogen) collisions [through the intranuclear-cascade-evaporation model<sup>6</sup> ( $E \leq 3$  GeV) and the extrapolation-evaporation model<sup>7</sup> ( $E \geq 3$  GeV)], nonelastic nucleon- and charged-pion-hydrogen collisions [via the isobar model<sup>8</sup> ( $E \leq 3$  GeV) and phenomenological fits to experimental data<sup>9</sup> ( $E \geq 3$  GeV)], elastic neutron-nucleus collisions ( $E \leq 100$  MeV), and elastic nucleon- and charged-pion collisions with hydrogen. In most applications using HETC, nucleons are transported to 15 MeV and charged pions are transported to  $\sim 2$  MeV, with negative pions being captured when they slow down to their cutoff energy. In spectrometer applications, neutrons below 15 MeV are assumed to deposit their energy at their point of origin. In applications where the transport of the low-energy neutrons is important, such as an ionization spectrometer in which fissionable material has been introduced, the three-dimensional multigroup neutron and gamma-ray Monte Carlo transport code MORSE<sup>10</sup> or the three-dimensional neutron Monte Carlo transport code O5R<sup>11</sup> is used.

The source distribution for the electromagnetic-cascade calculation, i.e. photons from neutral-pion decay, electrons and positrons from muon decay, and residual nuclear excitation energy, is provided by HETC. The transport of these particles is carried out by using a modified version of the Monte Carlo

code developed by Beck.<sup>12</sup> This code takes into account most of the significant electron-, positron-, and photon-interaction processes, i.e., Compton scattering, pair production, bremsstrahlung, photoelectric effect, annihilation, and the slowing down of electrons and positrons due to ionization and excitation.

The two major modifications of the original Beck code are: (1) the change from a one-medium transport code to a multimediuum transport code, and (2) the inclusion of a more generalized geometry package so that a three-dimensional transport calculation can be performed. For all processes except Compton scattering, however, the products of an interaction are assumed to be emitted in the same direction as the particle producing the interaction.

Gamma rays from the decay of excited nuclei following a nuclear interaction are not transported in the present spectrometer applications but are assumed to deposit their energy at their point of origin. This is a fairly good approximation since a large portion of the electromagnetic-cascade source energy for most problems considered results from neutral pions. Also, since most de-excitation photons are of low energy, they are rapidly absorbed by the media.

The nonlinearity of the light pulse (i.e., the light observed is not in direct proportion to the energy deposited due to saturation) has been taken into account by the use of Birks' law:<sup>13</sup>

$$\frac{dL}{dx} = \frac{dE/dx}{1+kB} \quad \text{or} \quad L(E_2) - L(E_1) = \int_{E_1}^{E_2} \frac{dE}{1+kB} \cdot \quad (1)$$

The light curves corresponding to several particles at low energies for the media indicated are shown in fig. 1 (a) for  $kB = 0.01 \text{ g/cm}^2/\text{MeV}$ . In the calculation, the light curves are extended to the maximum necessary energy.

The ionization energy loss,  $dE/dx$ , used in evaluating eq. 1, are taken from a program due to Armstrong and Chandler.<sup>14</sup> It is assumed that for electrons

---

and positrons a linear relation holds between the light observed and the energy deposited; i.e.,  $L = E$ . This is a very good approximation for all electron energies above 0.1 MeV.

In most applications, neutrons with energies  $< 15$  MeV are assumed to lose all their energy at their point of origin and to produce light in the scintillating material through proton recoil. Since low-energy neutrons produce a small fraction of the light observed in a nonfissionable medium, this is a good approximation. In addition, the light produced by the residual excitation energy which remains in a nucleus following a nuclear interaction and which is emitted in the form of gamma rays is assumed to be directly proportional to the energy available.

The Cerenkov response can be obtained from the following equations:

$$\frac{dI}{dx} = \frac{4\pi^2 e^2 Z^2}{hc^2} \Delta\nu \left(1 - \frac{1}{\beta^2 n^2}\right)$$

or

$$I = \int_{E_{\text{THRESHOLD}}}^E \frac{4\pi^2 e^2 Z^2}{hc^2} \Delta\nu \left(1 - \frac{1}{\beta^2 n^2}\right) \frac{dE}{dx} ,$$

where

$\frac{dI}{dx}$  = the number of photons emitted per centimeter,

$\Delta\nu$  = the frequency interval of the photons,

$Z$  = the charge of the particle,

$E_{\text{THRESHOLD}}$  = the threshold energy for emitting Cerenkov radiation,

$\beta$  = the velocity of the particle relative to light velocity  $c$ ,

$n$  = the index of refraction of the medium in the frequency interval considered,

$dE/dx$  = the ionization and excitation energy loss, and

$e, h, c$  = the electronic charge, Plank's constant, and the speed of

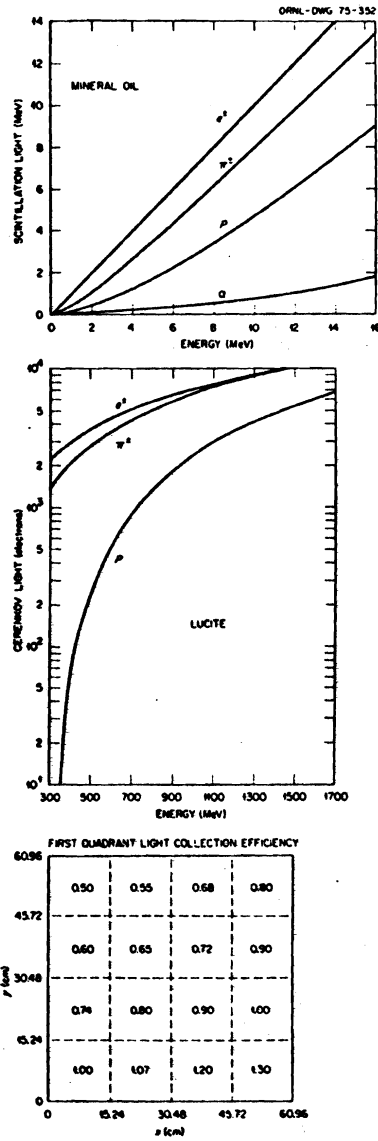


Fig. 1. (a) Scintillation light output vs charged-particle energy for several different types of particles. (b) Cerenkov light output vs charged-particle energy for several different types of particles. (c) First quadrant light collection efficiencies.

A group of Cerenkov radiation curves for the media indicated are shown in fig. 1 (b).  $\Delta\nu$  is taken to be  $2.9 \times 10^{14} \text{ sec}^{-1}$ , which corresponds roughly to the frequency range of the visible spectrum, and  $n$  is taken to be 1.5. Also, the number of photons has been converted to electrons by assuming an average photocathode efficiency in the  $\Delta\nu$  frequency range of 0.06, i.e., 0.06 electron/photon. Charged particles with  $A > 1$  are not considered since the number of these particles having energies above their Cerenkov threshold energies is negligible. The charged-muon response is not plotted but corresponds very closely to the curve for the charged pions. In the calculations, the Cerenkov radiation curves are extended from threshold to the maximum necessary energy.

The nonuniformity of light collection can be taken into account if experimental data for the particular device are available or if some reasonable estimates can be made. In fig. 1 (c), an example of the weighting factors for nonuniform light collection is given. Only the first quadrant is shown since the other three are assumed to be similar.

### III. CALCULATED DATA

The particular data presented here for two proto-type spectrometers designed by Selove and his collaborators<sup>15</sup> are indicative of some of the data which can be obtained calculationally. Only a small fraction of the total data calculated is presented.\*

The geometries of the mineral-oil-iron ionization spectrometers, hereinafter referred to as Design I and Design II, are given in Table 1. The basic difference between the two designs is that Design I, which has more active scintillation material, gives a slightly better sampling than does Design II.

---

\*A paper containing all the data is being prepared and will be available shortly.

Table 1  
Geometries of the 15-Cell Spectrometers  
Basic Cell

Design I		Design II	
Thickness (cm)	Material	Thickness (cm)	Material
0.32	Fe	0.32	Fe
3.81	Liquid Scintillator <sup>a</sup>	0.64	Dead Liquid Scintillator
1.27	Fe	0.64	Fe
3.81	Liquid Scintillator	4.45	Liquid Scintillator
1.27	Fe	2.54	Fe
3.81	Liquid Scintillator	4.45	Liquid Scintillator
0.32	Fe	0.64	Fe
		0.64	Dead Liquid Scintillator
		0.32	Fe

In both designs, 0.95 cm of Fe is placed in front of the first cell; between each of the 15 cells, there are:

0.71 cm Void  
1.91 cm Lucite<sup>b</sup>  
0.71 cm Void

In both designs, the lateral dimensions are 122 × 122 cm<sup>2</sup>.

a. Cl<sub>2</sub>, ρ = 0.87 g/cm<sup>3</sup>.

b. C<sub>3</sub>H<sub>8</sub>O<sub>2</sub>, ρ = 0.944 g/cm<sup>3</sup>.

In Design II, "dead liquid scintillator" means that no light pulse is collected from these sections.

In the experimental setup, 2.54 cm of wood was placed between each of the 15 cells instead of the lucite slabs used in the calculations. Lucite slabs are used in the calculations to obtain a sampling of the cascade by observing the resulting Cerenkov radiation.

A summary of the energy deposition and leakage energy when 7-GeV/c protons are incident on the Design II spectrometer is given in Table 2. The saturation effect is quite apparent by comparing the linear and nonlinear columns in the table. The average Cerenkov pulse height from the 14 lucite slabs is given in Table 3. As can be seen, the electromagnetic contribution dominates this pulse height. The scintillation pulse-height distribution and the Cerenkov pulse-height distribution are given in fig. 2. The experimental scintillation pulse-height distribution is well predicted by the calculations.

Correlations between the scintillation (nonlinear) pulse height and the Cerenkov pulse height, the linear minus nonlinear pulse height and the Cerenkov pulse height, and the binding energy plus neutrino energy and the Cerenkov pulse height are given in fig. 3 (a), (b), and (c), respectively, for 7-GeV/c protons incident on the Design I spectrometer. As indicated in the figure, a large scintillation pulse height usually requires a large Cerenkov pulse height, and a large binding energy plus neutrino energy requires a small Cerenkov pulse height. This is as expected since a large scintillation pulse height has a large electromagnetic contribution which

Table 2  
Energy Deposition and Leakage Energy Produced by the Interaction  
of 7-GeV/c Protons in the Design II Spectrometer<sup>a</sup>

Type of Energy Deposition	Energy Deposition (MeV)			
	Iron, Lucite, and Liquid (linear)	Liquid		
		Nonlinear Nonuniform Light	Linear	Nonlinear <sup>b</sup>
Primary ionization	178.	35.1	35.8	35.1
Secondary proton ionization	2042.	372.	492.	390.
Secondary $\pi^{\pm}$ ionization	520.	106.	115.	111.
Secondary $\mu^{\pm}$ ionization	10.4	1.90	2.31	2.24
Nuclear recoil and evaporated charged particles other than protons <sup>c</sup>	171.	6.89	51.4	7.11
Excitation energy following evaporation <sup>c</sup>	139.	18.4	19.8	19.8
Neutrons with energy < 10 MeV <sup>c</sup>	184.	13.7	39.4	14.7
Electromagnetic	1165.	228.	235.	235.
Total	4409.	782.	991.	815.

Particle Type	Leakage Energy (MeV)		
	Front	Side	Back
Protons	4.82	18.0	72.2
Neutrons	51.7	264.	110.
$\pi^{\pm}$ d	19.6	19.7	27.6
$\mu^{\pm}$ d	0.	1.32	0.85
$\gamma$	16.4	15.3	7.33
$e^{\pm}$ d	5.26	2.23	1.35
Total	97.8	321.	219.

Total leakage energy (MeV)	638.
Binding plus neutrino energy (MeV)	1074.
Electromagnetic source energy (MeV)	1215.

a. See description of spectrometer.

b.  $kB = 0.01 \text{ g/cm}^2/\text{MeV}$ .

c. Assumed to deposit their energy at their point of origin.

d. Includes rest mass.

**Table 3**  
Average Cerenkov Pulse Height Produced by the Interaction  
of 7-GeV/c Protons in the Design II Spectrometer

	Average Cerenkov Pulse (electrons)
Primary particles	45.6
Secondary protons	73.4
Secondary charged pions	123.
Secondary muons	2.2
Electromagnetic cascade	<u>331.</u>
<b>Total</b>	<b>575.</b>

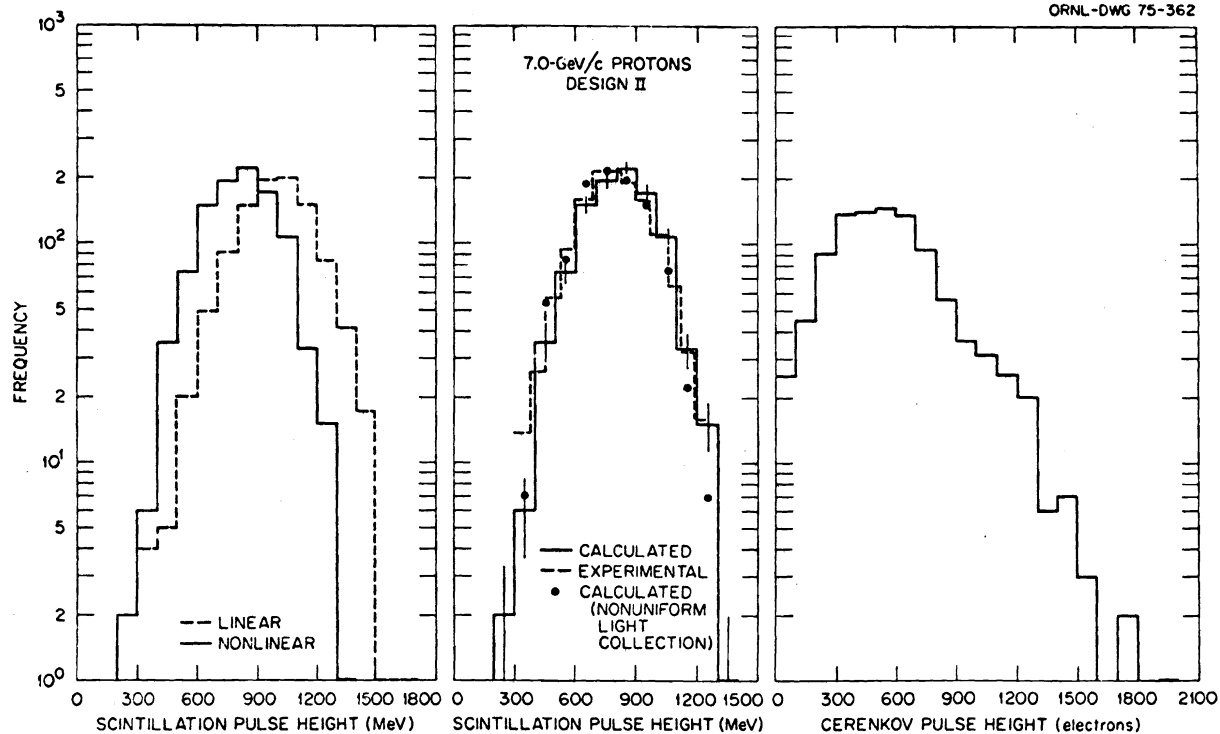


Fig. 2. Linear and nonlinear scintillation pulse-height distributions in Design II for incident protons of momentum 7 GeV/c; a comparison between the calculated and experimental pulse-height distributions (also shown is the effect of including nonuniform light collection); and Cerenkov pulse-height distribution.

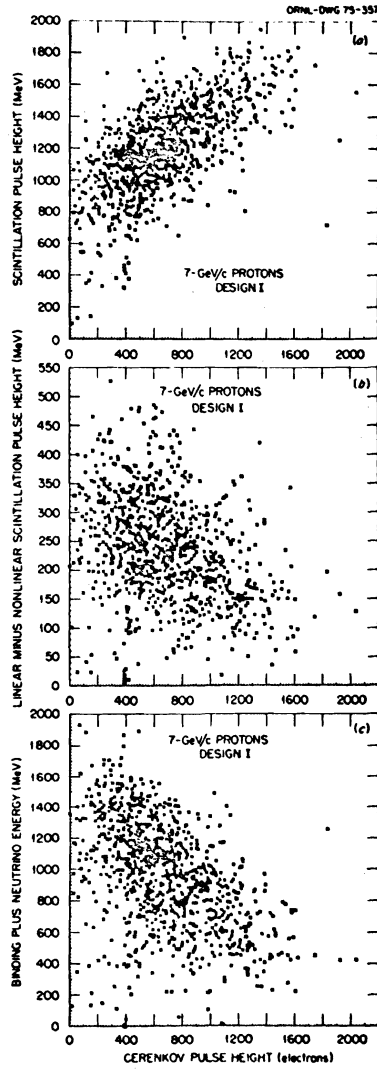


Fig. 3. (a) Scintillation pulse height vs Cerenkov pulse height in Design I for incident protons of momentum 7 GeV/c. (b) Linear minus nonlinear scintillation pulse height vs Cerenkov pulse height. (c) Binding-plus-neutrino energy vs Cerenkov pulse height.

leads to a large Cerenkov pulse height. Also, since a large loss of energy due to binding energy or to neutrinos leads to a smaller electromagnetic contribution, one would expect a smaller Cerenkov pulse height.

The expected scintillation pulse-height distributions for 7-GeV/c protons, negative pions, and electrons incident on the Design II spectrometer, as well as the average visible scintillation energy vs the energies of the incident particles for the three particle types considered for the Design I spectrometer are shown in fig. 4.

ORNL-DWG 75-370

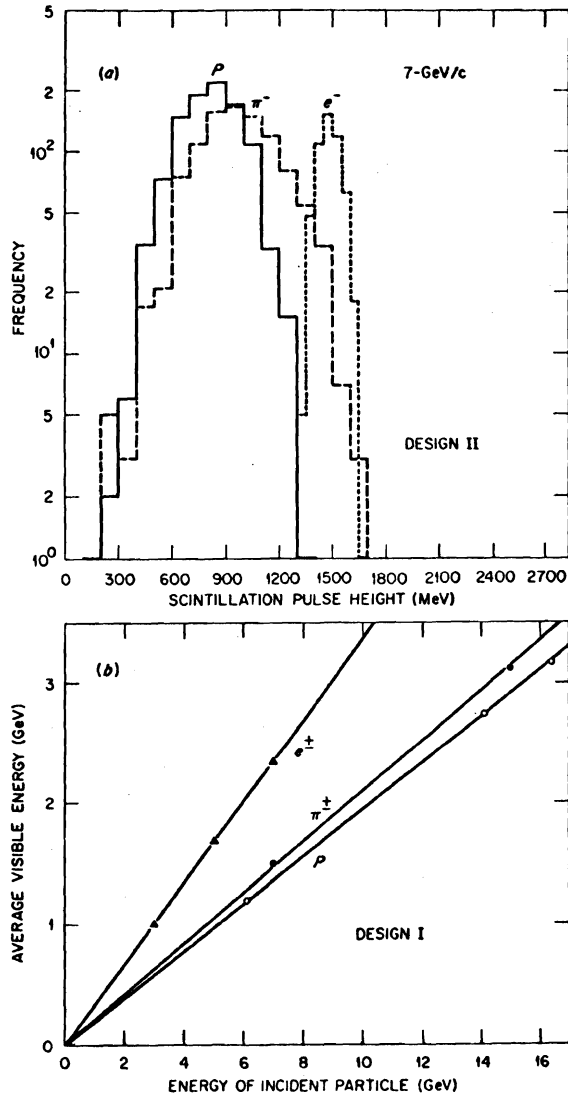


Fig. 4. (a) A comparison of the pulse-height distributions in Design II for the three particle types, p,  $\pi^-$ , and  $e^-$ , at a momentum of 7 GeV/c. (b) Average visible energy vs energy of the incident particles for Design I.

REFERENCES

- 1) V. S. Murzin, Principles and application of the ionization chamber calorimeter, in Progress in Elementary Particle and Cosmic-Ray Physics (J. G. Wilson and S. A. Wouthuysen, ed., North-Holland Publishing Co., Amsterdam, 1967).
  - 2) W. J. Willis and V. Radeka, Nucl. Instr. Meth. 120 (1974) 221.
  - 3) T. A. Gabriel and J. D. Amburgey, Nucl. Instr. Meth. 116 (1974) 333.
  - 4) T. A. Gabriel and K. C. Chandler, Particle Accelerators 5 (1973) 161.
  - 5) K. C. Chandler and T. W. Armstrong, Operating instructions for the high-energy nucleon-meson transport code HETC, ORNL-4744, Oak Ridge National Laboratory (1972).
  - 6) H. W. Bertini, Phys. Rev. C 6 (1972) 631.
  - 7) T. A. Gabriel, R. G. Alsmiller, Jr., and M. P. Guthrie, An extrapolation method for predicting nucleon and pion differential production cross sections from high-energy (> 3 GeV) nucleon-nucleus collisions, ORNL-4542, Oak Ridge National Laboratory (1970).
  - 8) Hugo W. Bertini, Miriam P. Guthrie, and Arline H. Culkowski, Phenomenologically determined isobar angular distributions for nucleon-nucleon and pion-nucleon reactions below 3 GeV, ORNL-TM-3152, Oak Ridge National Laboratory (1970).
  - 9) T. A. Gabriel, R. T. Santoro, and J. Barish, A calculational method for predicting particle spectra from high-energy nucleon and pion collisions ( $\approx$  3 GeV) with protons, ORNL-TM-3615, Oak Ridge National Laboratory (1971).
  - 10) E. A. Straker *et al.*, The MORSE code - a multigroup neutron and gamma-ray Monte Carlo transport code, ORNL-4585, Oak Ridge National Laboratory (1970).
-

- 11) D. C. Irving *et al.*, OSR, a general-purpose Monte Carlo neutron transport code, ORNL-3622, Oak Ridge National Laboratory (1965).
- 12) H. L. Beck, A Monte Carlo simulation of the transport of high energy electrons and photons in matter, HASL-213, USAEC Health and Safety Laboratory (1969).
- 13) J. B. Birks, The Theory and Practice of Scintillation Counting (The Macmillan Company, New York, 1964).
- 14) T. W. Armstrong and K. C. Chandler, SPAR, a FORTRAN program for computing stopping powers and ranges for muons, charged pions, protons, and heavy ions, ORNL-4869, Oak Ridge National Laboratory (1973).
- 15) "Performance of a Sampling Calorimeter at 3 to 17 GeV, a Preliminary Report," BNL-PENN-WISCONSIN, University of Pennsylvania Internal Report, October 15, 1973.